Experimental Study on the Mixing of One- and Dual-Line Heated Jets with a Cold Crossflow in a Confined Channel

K. S. Chen* and J. Y. Hwang†
National Sun Yat-Sen University, Kaohsiung, Taiwan, Republic of China

An experimental study is presented for the mixing of one- and dual-line heated jets injected normally into a cold crossflow in a rectangular channel. Measurements of the mean temperature, velocity, and turbulence intensity together with the flow visualization were performed. Self-similar forms for the dimensionless vertical temperature profiles were found. Parametric variations characterizing the mixing processes of the temperature and velocity fields were examined and correlated in terms of the momentum flux ratio and downstream distance. Results show that both the thermal and velocity penetration depths increase with increasing momentum flux ratio and downstream distance. The turbulence intensity is strong within the region of jet half-width, and the maximum value occurs at a point close to the jet velocity trajectory.

Nomenclature

a = speed of sound
B = duct width; see Fig. 2
D = jet nozzle width
H = duct height; see Fig. 2
J = momentum flux ratio, $=(\rho_j V_j^2)/(\rho_\infty U_\infty^2)$
M = Mach number, $=U/a$
$\bar{T}$ = mean temperature
T_j = jet temperature at the nozzle exit
T_∞ = mainstream temperature
$\bar{U}$ = mean velocity in the X direction
$\tilde{U}$ = dimensionless velocity difference ratio defined in Eq. (2)
$\bar{u}'$ = mean turbulent velocity component in the X direction
V_j = jet velocity at nozzle exit
$W^{\pm\frac{1}{2}}$ = plus or minus jet half-width; see Fig. 2
X = horizontal coordinate; see Fig. 2
Y = vertical coordinate; see Fig. 2
Y_c = jet circulation depth; see Fig. 2
Y_T = jet thermal penetration depth; see Fig. 2
Y_v = jet velocity penetration depth; see Fig. 2
Z = spanwise coordinate; see Fig. 2
θ_c = dimensionless temperature difference ratio defined in Eq. (1)
ρ_∞ = mainstream density
ρ_j = jet density
σ = percentage root-mean-square deviation

Introduction

THE penetration and the mixing characteristics of a cooling (or heated) jet injected normally into a heated (or cooled) crossflow have important engineering applications, particularly pertaining to the dilution zone design in gas turbine combustors and the lifting jets for very short takeoff and landing (V/STOL) aircrafts. Extensive researches have been given on the mixing process of single heated jet injected into a cool crossflow[1-4] and of the multiple cool jets injected in a heated crossflow.[6-8] Cox[7] and Holdeman and Walker[8] presented comprehensive empirical models and correlations for predicting the temperature distributions and relevant parametric variations downstream of a row of cool jets injected normally to a hot confined crossflow. It was found[5-8] that the most important independent flow variable was the momentum flux ratio, and the density (or temperature) ratio need not be considered. However, there are no experimental data available that could be used for predicting dual side dilution configurations.[8]

The present work presents an experimental study on the mixing characteristics of one- and dual-line heated jet injected normally into a cold crossflow in a rectangular duct of constant cross-sectional area. The objective of this study is 1) to quantify the parametric variations characterizing the mixing of one- and dual-line heated jets with cold crossflow; and 2) to provide a two-dimensional data base of the dilution-jet mixing for the analytical and/or numerical analysis and turbulence modeling. Detailed temperature and velocity measurements were made by thermocouple probes and laser-Doppler velocimeter (LDV). Flow visualization by dye injection was also performed. Correlations of the parametric variations such as the temperature and velocity trajectories, circulation depth, and jet half-width in terms of the momentum flux ratio and the downstream distance are presented and discussed.

Test Apparatus, Procedures, and Conditions

The main parts of the test facility consisted of one cold-air channel, two ducts and nozzles for the heated jets, three blowers and frequency converters, and one power control panel, as shown in Fig. 1. Detailed descriptions on the test apparatus and procedures are available in Chen et al.[9] Consequently, only brief summaries are given.

Ambient air ($T_\infty \simeq 25°C$) was supplied from one blower to the rectangular channel made of 2-mm-thick steel strip with a cross-sectional area of 120×240 mm^2. The test section was 300 mm long and was 800 mm downstream of the straightener section. The two sides of the test section were made of 3-mm-thick quartz glass to allow LDV measurements and flow visualization. The straightener section was 72 mm long and was 1250 mm downstream of the blower exit. The honeycomb in the straightener section was netted by acrylic bars as shown in Fig. 1. Note that the lengths of the rectangular channel and the straightener section and the distances between each section were designed according to the American Society of Heating, Refrigeration and Air Conditioning Engineering (ASHRAE) and American Motor Corporation Association (AMCA) standards.[10] In the experiment on one-line (bottom) heated jet, the nozzle opening of the top jet was sealed by the plastic tape.

Two identical rectangular nozzle slots were flush-mounted on the top and bottom sides in the test section. In order to

Received July 20, 1989; revision received Nov. 27, 1989.

*Associate Professor, Institute of Applied Mechanics.
†Graduate Student, Department of Mechanical Engineering.

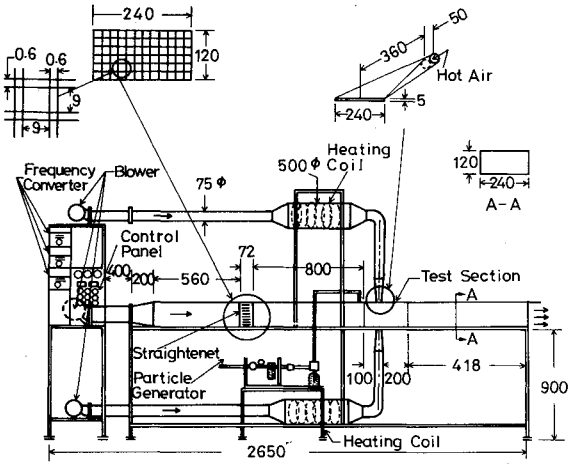

Fig. 1 Schematic of test apparatus.

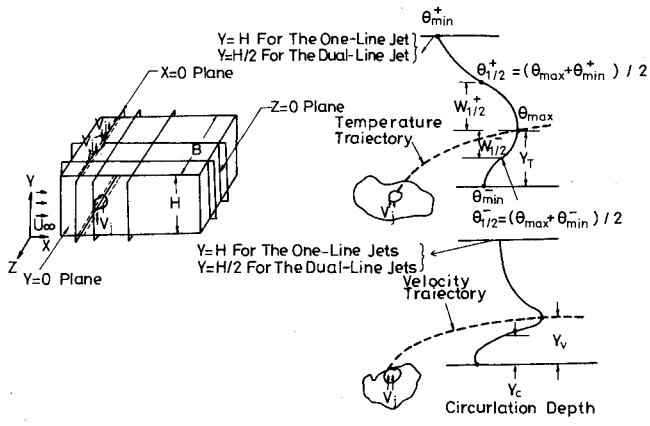

Fig. 2 Coordinate system and relevant parameters characterizing the vertical temperature and velocity profiles.

simulate a two-dimensional flowfield, each nozzle had an opening ratio of 48 (=240/5) and had an enlarged and wedge-type passage, as shown in Fig. 1. Measurements of the velocity and temperature profiles in the spanwise (Z) direction were carried out to check the uniformity. These measurements showed that the thermal and flowfields exhibited good two dimensionality in the spanwise direction away from the side walls. Ambient air was supplied to each of the heating coils by the blower and was injected into the test section through the nozzle opening with width $D = 5$ mm. The electrical voltages to the heating coils could be adjusted manually on the power control panel. The speeds of the jets or crossflow could be varied by adjusting individually the rotation speed of each blower up to 3600 rpm. The adjustment was done on each frequency converter operating in the range of 0–60 Hz with a 0.5-Hz increment in the digital reading. Every change of 1 Hz in the frequency converter corresponded to a change of 60 rpm in the rotation speed of the blower.

Measurements of the mean velocity and turbulence components in the X direction were made with a one-component LDV system operating in a forward-scattering, dual-beam mode. The principal components used in the LDV system were a Spectra-Physics 3W argon-ion laser (green light), a Dantec 55X-series one-color optical assembly (including a 40-MHz Bragg cell), a frequency counter, a frequency shifter, and an RCA photomultiplier. The laser and the optical components were mounted on an optical table, which was equipped with X-, Y-, Z-traversing mechanisms. The movement of the table in each direction was controlled by an ac motor, which was interfaced to a 16-bit personal computer for data acquisition, storage, and reduction. A 600-mm focus length achromat formed the probe volume with a waist diameter of approximately 0.1 mm. Calibration of the LDV system was performed by comparing the output signal recorded from a stationary scatterer with that obtained directly from the differential signal of the optical-electronic shifter. These calibrations were typically in agreement to within 5 Hz, corresponding to a velocity of 10 μ/s.

Seeding of the flow for the LDV measurement was done by a particle generator, which consisted of an air compressor, a TSI 3074 air filter, and a TSI 3076 constant-output atomizer. Particles from the glycerol-water mixture with diameters of 0.1–1 μ were fed into the main stream using a 5-mm-diam plastic tube through the hole on the top wall of the channel at a distance about 400 mm upstream of the test section. The typical data rate was 10–50 kHz, with a validation rate of approximately 30–60%. A minimum of 1000 frequency samples were recorded for each measurement from which mean and turbulent components were calculated from the ensemble (or unweighted) average. As noted by Johnson et al.[11] for the individual-realization mode of laser velocimetry, the error associated with the sampling bias of the first-order mean was approximately equal to the square of turbulent intensity and was independent of the data rate for the dilute seeding. Also, they found that the differences in the weighted and unweighted results were not large in the second-order turbulent quantities.[11] In this study the turbulent intensity was found to be less than 30% for most regions of the flow, and the maximum value (about 40%) was only confined in the vicinity of the jet trajectory. Accordingly, the bias error in the LDV measurement would be within 10% for most cases of the mean velocity components.

The average speed of the cooling air in the duct or the jet velocity at the nozzle exit was measured by a Testovent 4300 vane anemometer with digital readout. Calibration curve of the vane anemometer readings (m/s) against the frequency outputs (Hz) from the frequency converter for each blower was first established and then used for the subsequent measurements. A check was made by comparing the LDV data with the vane anemometer measurement, which showed very good agreements (less than 3% deviation).

Average temperatures of the flow were measured by Omega Type-K thermocouple wires of 2 mm diam. Twelve equally spaced wires were mounted on a rake. The rake was made of 1-mm-thick, 120-mm-high aluminum plate with twelve holes in it, and was placed against the top and bottom walls inside the channel. Once the temperature measurements at one cross section had been completed, one side window was removed and the rake was manually placed to the next section. The side window was then put back and the new data were taken after all of the temperature readings remained essentially unchanged. All thermocouple wires were connected to an HEW 3088 data logger with automatic ambient compensation. Calibration of the thermocouple wires in a well-mixed ice box showed a maximum error of about ±0.3°C. Notice that the thermocouple rake arranged in this study (also in Callagan and Ruggeri[1]) measured the total temperature actually. However, for all measurements in this study M was less than 0.04. Consequently, the compressibility effect (proportional to M^2) was negligible, and the total temperature was essentially equal to the static temperature.

Flow visualization was done by injecting the smoke of the burning incense into the flow. A bundle of incense was placed inside a container that was connected by plastic tubes, respectively, to an air compressor and an injector. The injector was made with a tube 120 mm long and with 12 mm i.d. There were 17 holes of 4 mm diam equally spaced on the tube. The injector was placed against the top and bottom walls inside the duct at a location about 400 mm upstream of the test section. A 500-W slide projector was used as the light source. Light was shined into the flow from the channel exit. A piece of black paper was placed in front of the light source to form a light sheet. Snapshots were taken with Konica SR-V-3200 films at 0.1-s exposure time for most cases.

Table 1 Conditions for temperature measurements

T_j, °C	T_∞, °C	V_j, m/s	U_∞, m/s	ρ_j/ρ_∞	J
41.0	22.7	17.4	2.18	0.942	60.0
41.9	22.7	17.4	2.37	0.940	50.6
56.2	22.5	17.4	2.60	0.900	40.3
62.0	22.2	13.9	2.37	0.881	30.3
80.2	21.4	13.0	2.37	0.833	25.0
108.5	22.4	12.0	2.37	0.774	19.8
124.5	22.4	9.87	2.18	0.743	15.2

Table 2 Conditions for velocity measurements

T_j, °C	T_∞, °C	V_j, m/s	U_∞, m/s	ρ_j/ρ_∞	J
41.9	23.5	17.4	2.37	0.942	50.4
56.2	23.0	17.4	2.60	0.899	40.2
70.0	24.5	13.9	2.18	0.856	34.9
60.1	24.5	13.9	2.37	0.896	30.4
75.0	24.0	13.0	2.37	0.853	25.2

All results presented for the velocity and temperature measurements were carried out on the central plane ($Z = 0$ plane). The origin 0 is placed at the bottom and at the central plane of the nozzle opening. The coordinate system and relevant parameters characterizing the mixing processes are depicted in Fig. 2. Note that, as will be seen later, the velocity and temperature profiles for the dual-line jets are symmetric about the channel midheight $Y = H/2$. Therefore, only the lower half of the profile for the case of the dual-line jets needs to be considered.

The experimental conditions for the temperature and velocity measurements are listed in Tables 1 and 2, respectively, and cover the ranges of

$$15.2 \le J\left(=\frac{\rho_j V_j^2}{\rho_\infty U_\infty^2}\right) \le 60$$

$$1.05 \le \frac{T_j}{T_\infty} \le 1.36$$

$$3.79 \le \frac{V_j}{U_\infty} \le 8.0$$

$$0.743 \le \frac{\rho_j}{\rho_\infty} \le 0.942$$

Measurements were carried out at various X planes ranging from $2 \le X/D \le 10$. Note that in the data reduction only the variables J and X/D were used as the independent parameters, and others were not considered. The results for the temperature and velocity profiles are presented as the dimensionless difference ratios according to

$$\theta = \frac{\bar{T} - T_\infty}{T_j - T_\infty} \tag{1}$$

$$\tilde{U} = \frac{\bar{U} - U_\infty}{U_{\max} - U_\infty} \tag{2}$$

where T and U are the average temperature and velocity at the measuring location, and $U_{\max}$ the maximum velocity at a given cross section.

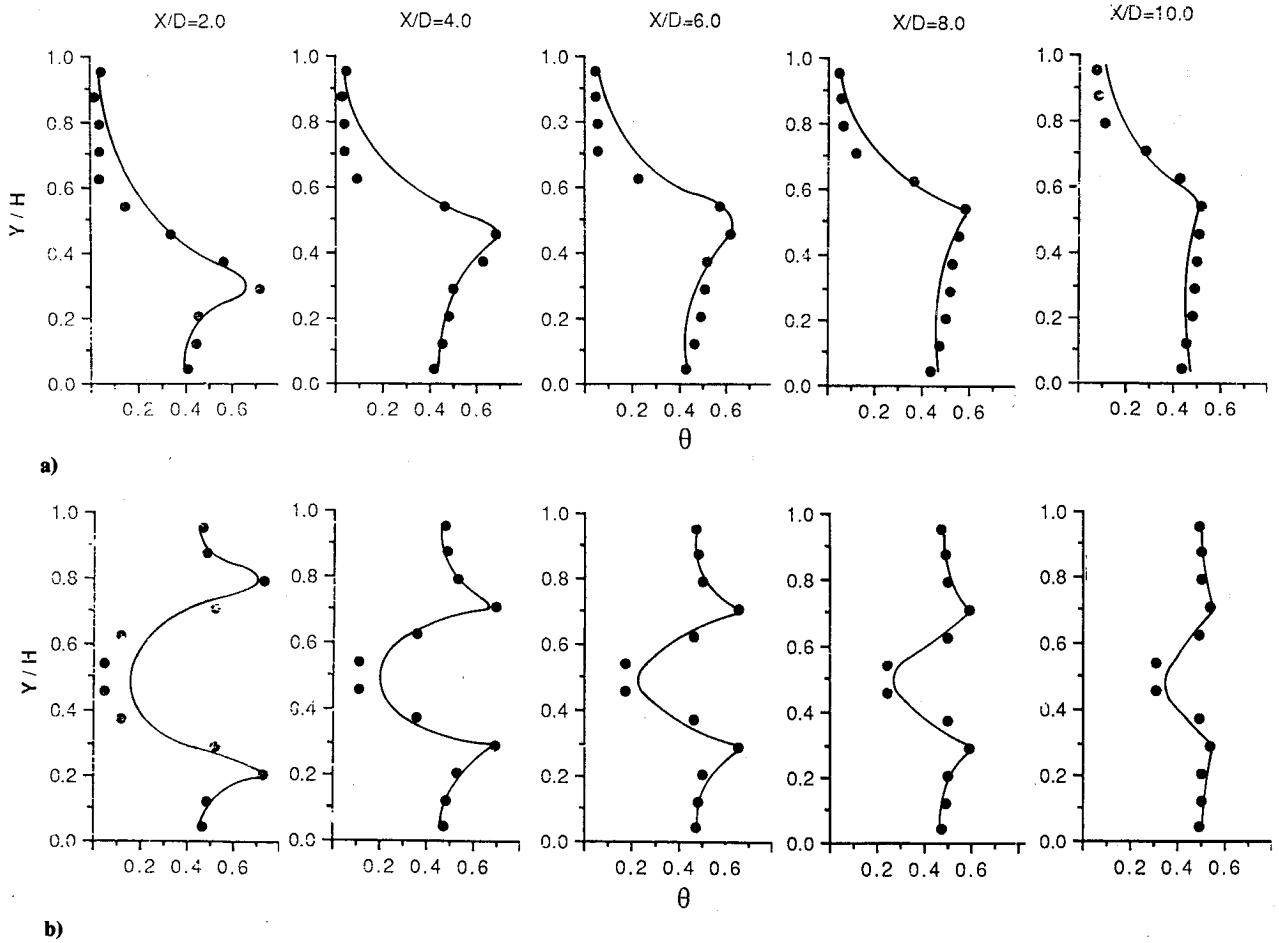

Fig. 3 Temperature profiles at $J = 25.0$: a) for one-line jet; b) for dual-line jets.

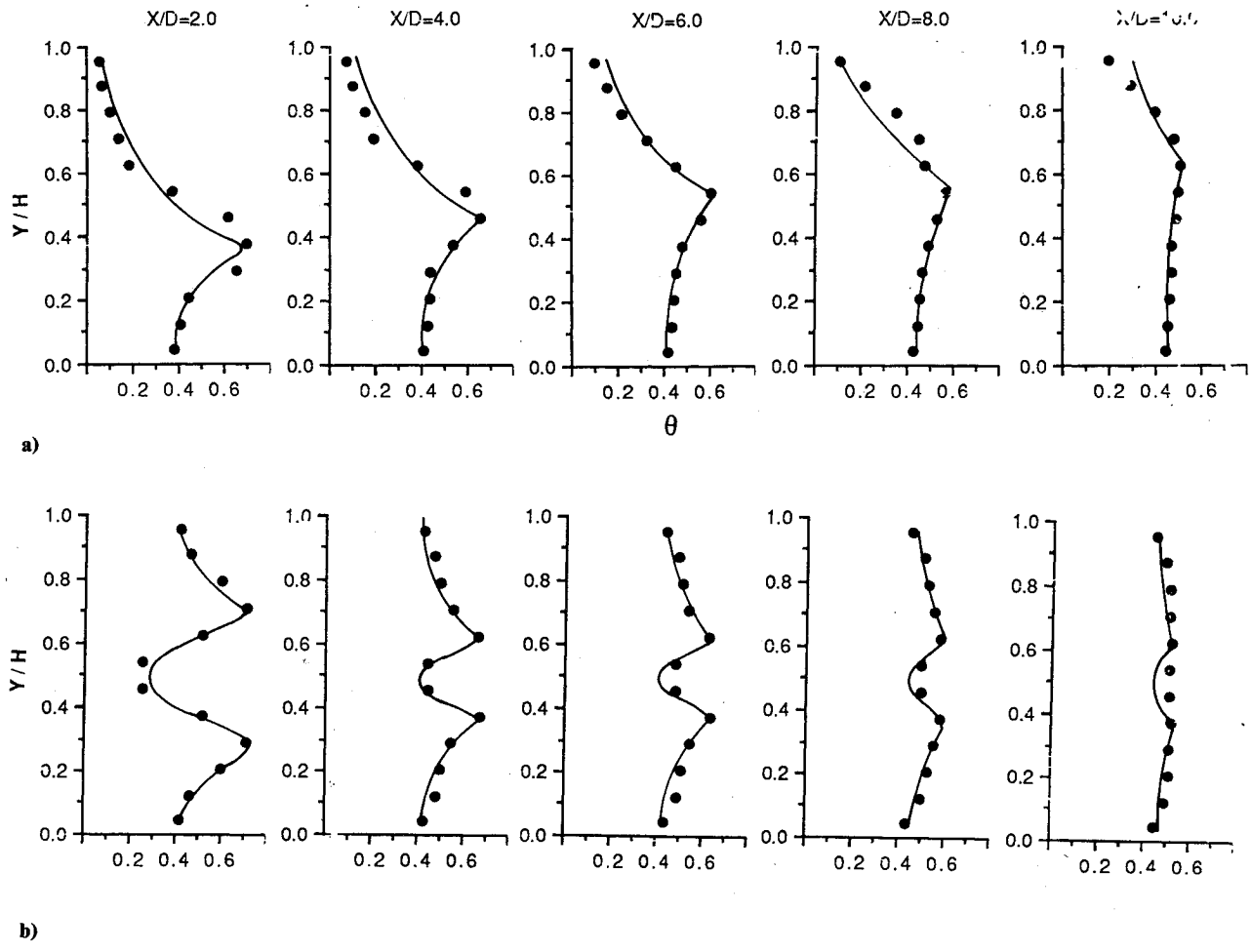

Fig. 4 Temperature profiles at $J = 50.6$: a) for one-line jet; b) for dual-line jets.

Results and Discussion

Temperature Field

Typical vertical temperature profiles at various X planes are shown in Figs. 3 and 4 for the momentum flux ratios $J = 25.0$ and 50.6, respectively. In each figure part a is for the case of one-line (bottom) jet and part b is for the dual in-line jets.

It is seen from Figs. 3a and 4a for the one-line jet that the temperature of the mixing air at a fixed X/D plane increases from the nozzle exit with the increasing height Y/D to a maximum value and decreases monotonically thereafter. Because of the energy exchange of hot jet with cold crossflow, the position of the maximum temperature (or temperature trajectory), Y_T/D, at each cross section moves away from the jet side with the downstream distance. As the momentum flux ratio increases, Y_T/D and $W^{\pm}_{1/2}$ also increase.

For the dual-line jets shown in Figs. 3b and 4b, temperature distribution is almost symmetric about the duct mid-height point $Y/H = 0.5$ at every X/D plane (within the experimental uncertainty), where $\theta = \theta_{\min}$. For the lower half of the temperature field the jet temperature penetration depth Y_T/D, where $\theta = \theta_{\max}$, also increases with increasing X/D and J.

The following self-similar forms for the previously given temperature profiles can be found:

$$\frac{\theta - \theta^{\pm}_{\min}}{\theta_{\max} - \theta^{\pm}_{\min}} = C_1 \exp\left[-C_2 \left(\frac{\frac{Y}{H} - \frac{Y_T}{H}}{\frac{W^{\pm}_{1/2}}{H}} \right)^2 \right] \tag{3}$$

where for a one-line jet $C_1 = 0.573$ and $C_2 = 0.215$ and for dual-line jets $C_1 = 0.448$ and $C_2 = 1.0$.

Table 3 Correlation equations for one-line jet

Y_T/D	$3.444J^{0.192}(X/D)^{0.311}$	$\sigma = \pm 20.5\%$
$\theta^{+}_{\min}/\theta_{\max}$	$\frac{1-e^{-c+}}{C^+ = 0.00038J^{1.52}(X/D)^{0.202}}$	$\sigma = \pm 19.6\%$
$\theta^{-}_{\min}/\theta_{\max}$	$\frac{1-e^{-c-}}{C^- = 2.094J^{-0.320}(X/D)^{0.416}}$	$\sigma = \pm 21.4\%$
$W^{+}_{1/2}/D$	$1.36J^{0.16}(X/D)^{0.273}$	$\sigma = \pm 16.7\%$
$W^{-}_{1/2}/D$	$0.756J^{0.145}(X/D)^{0.368}$	$\sigma = \pm 18.9\%$
Y_v/D	$1.783J^{0.297}(X/D)^{0.42}$	$\sigma = \pm 15.8\%$
Y_c/D	$1.407J^{0.252}(X/D)^{0.512}$	$\sigma = \pm 22.6\%$

Table 4 Correlation equations for dual-line jets

Y_T/D	$2.145J^{0.289}(X/D)^{0.196}$	$\sigma = \pm 27.0\%$
$\theta^{+}_{\min}/\theta_{\max}$	$\frac{1-e^{-c+}}{C^+ = 0.172J^{-0.032}(X/D)^{1.183}}$	$\sigma = \pm 14.9\%$
$\theta^{-}_{\min}/\theta_{\max}$	$\frac{1-e^{-c-}}{C^- = 0.078J^{0.711}(X/D)^{0.054}}$	$\sigma = \pm 18.6\%$
$W^{+}_{1/2}/D$	$0.738J^{0.12}(X/D)^{0.553}$	$\sigma = \pm 22.3\%$
$W^{-}_{1/2}/D$	$0.6J^{0.15}(X/D)^{0.407}$	$\sigma = \pm 20.5\%$
Y_v/D	$2.232J^{0.159}(X/D)^{0.42}$	$\sigma = \pm 22.3\%$
Y_c/D	$1.495J^{0.184}(X/D)^{0.441}$	$\sigma = \pm 24.8\%$

In the Eq. (3) $\theta_{\max}$, $\theta^{\pm}_{\min}$, Y_T/H, and $W^{\pm}_{1/2}/H$ are the scaling parameters, as shown in Fig. 2. Equation (3) is expressed by the solid lines in Figs. 3 and 4. It is seen that the correlations

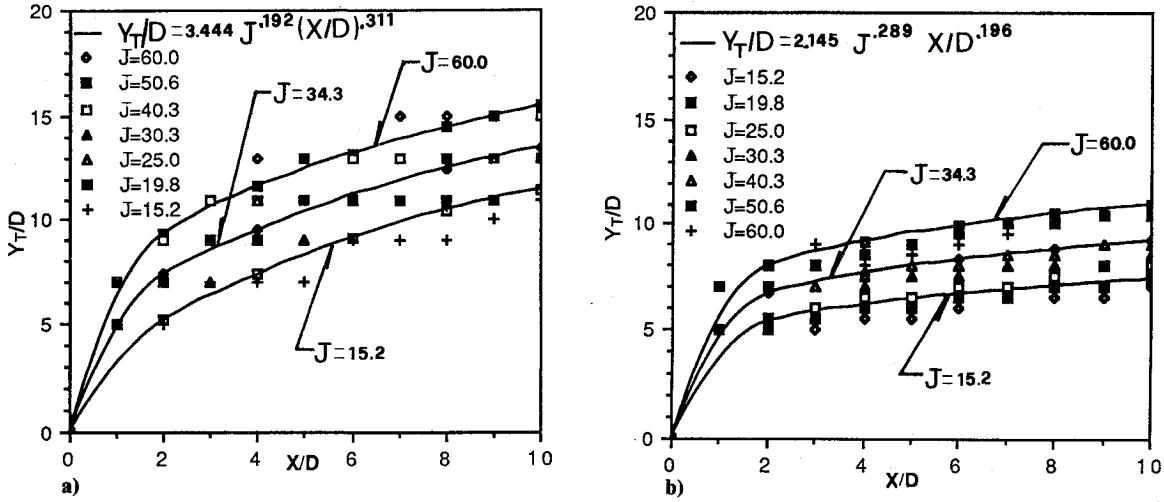

Fig. 5 Correlations of jet temperature trajectory: a) for one-line jet; b) for dual-line jets.

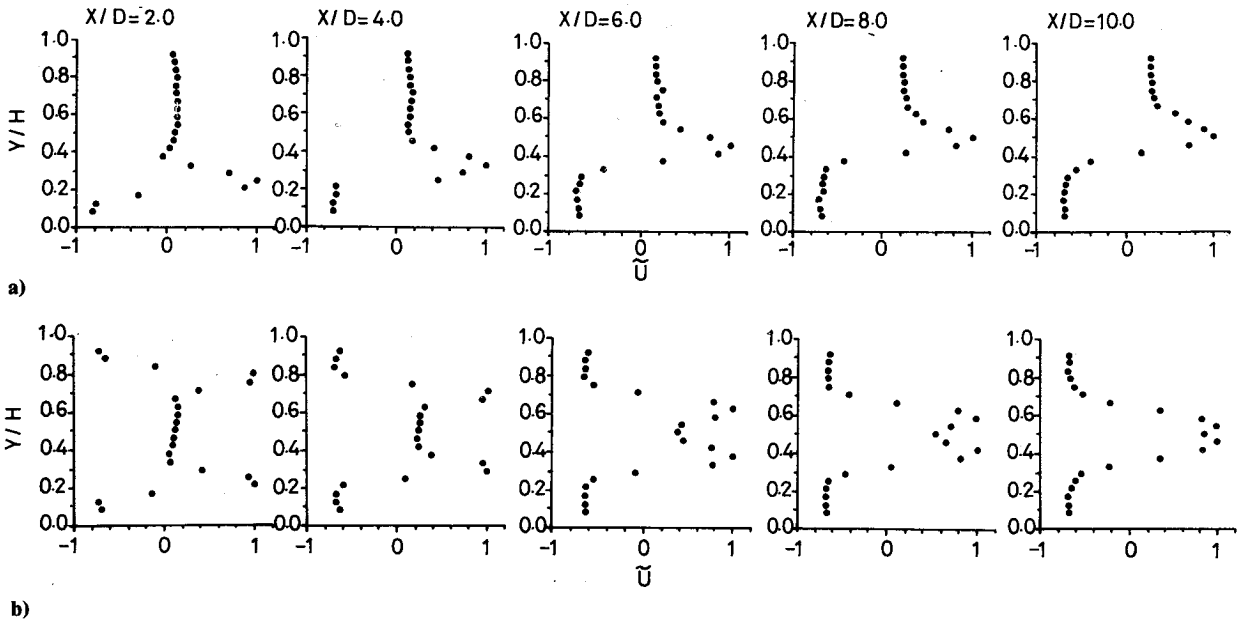

Fig. 6 Velocity profiles at $J = 25.2$: a) for one-line jet; b) for dual-line jets.

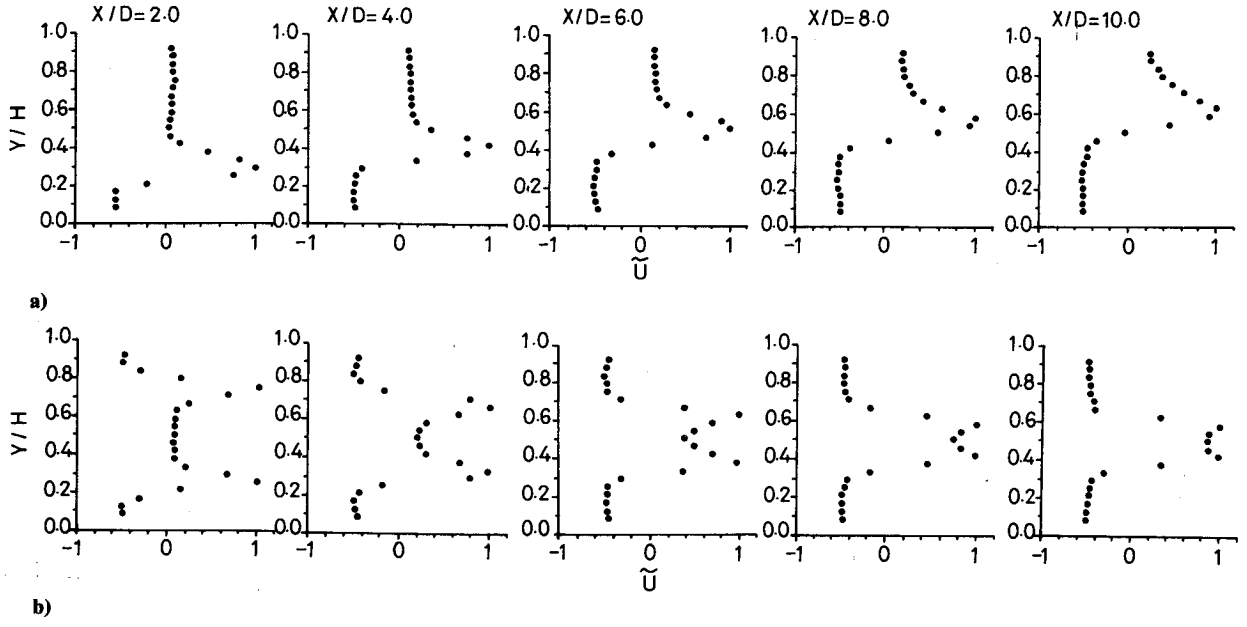

Fig. 7 Velocity profiles at $J = 50.4$: a) for one-line jet; b) for dual-line jets.

fit the data fairly well. The root-mean-square deviation between the correlation and the data is within 10.5%. Note that the self-similar forms for the dimensionless temperature profiles were also observed by Holdeman and Walker[8] in the mixing of a row of jets with a confined crossflow with $C_1 = 1$ and $C_2 = \ell n 2$ in Eq. (3).

From these temperature profiles various dependent or scaling parameters characterizing the thermal field can also be obtained in terms of the independent flow and geometric variables. These include the jet temperature trajectory (or thermal penetration depth), Y_T, the plus- and minus-minimum temperature $\theta^{\pm}_{\min}$, and $W^{\pm}_{1/2}$, as depicted in Fig. 2. Notice that, for a one-line (bottom) jet, "minus" refers to the jet side and "plus" refers to the opposite side. For the dual-line jets, since the temperature profile at every X/D plane is symmetric about the midheight point, only the lower-half portion ($0 \le Y/H \le 0.5$) is considered.

Tables 3 and 4 list the resulting correlations of these dependent parameters in terms of the independent variables J and X/D by using the least-squares regression method for one-line and dual-line jets, respectively. Typical correlation curves for the jet temperature trajectories are shown in Figs. 5a and 5b. It is seen from Figs. 5a and 5b that the jet temperature trajectories appear to be parabolic lines. It can be seen from Tables 3 and 4 that $W^{\pm}_{1/2}$ also increases with increasing J and X/D. The last column in Tables 3 and 4 represents the $\sigma\%$ of the correlation from the measurement data. It ranges from 14 to 28%.

Velocity Field

Typical mean vertical velocity profiles at various X planes are depicted in Figs. 6 and 7 for the momentum flux ratios $J = 25.2$ and 50.4, respectively. For the one-line jet shown in Figs. 6a and 7a the dimensionless velocity difference ratio U at a fixed X/D plane is negative near the nozzle exit region; that is, the horizontal velocity of the mixing air is smaller than U_∞ and exhibits a recirculation zone near the nozzle exit. The velocity profile at every X/D plane also shows that there is a zero-crossing point, Y_c, at which U changes from a negative value to a positive one. The value of Y_c is the

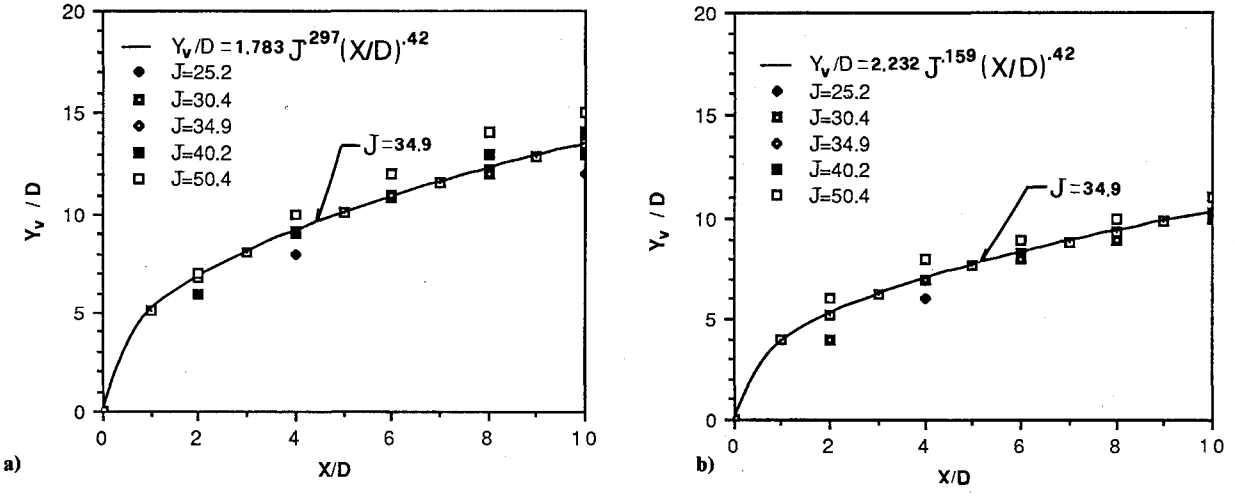

Fig. 8 Correlations of jet velocity trajectory: a) one-line jet; b) dual-line jets.

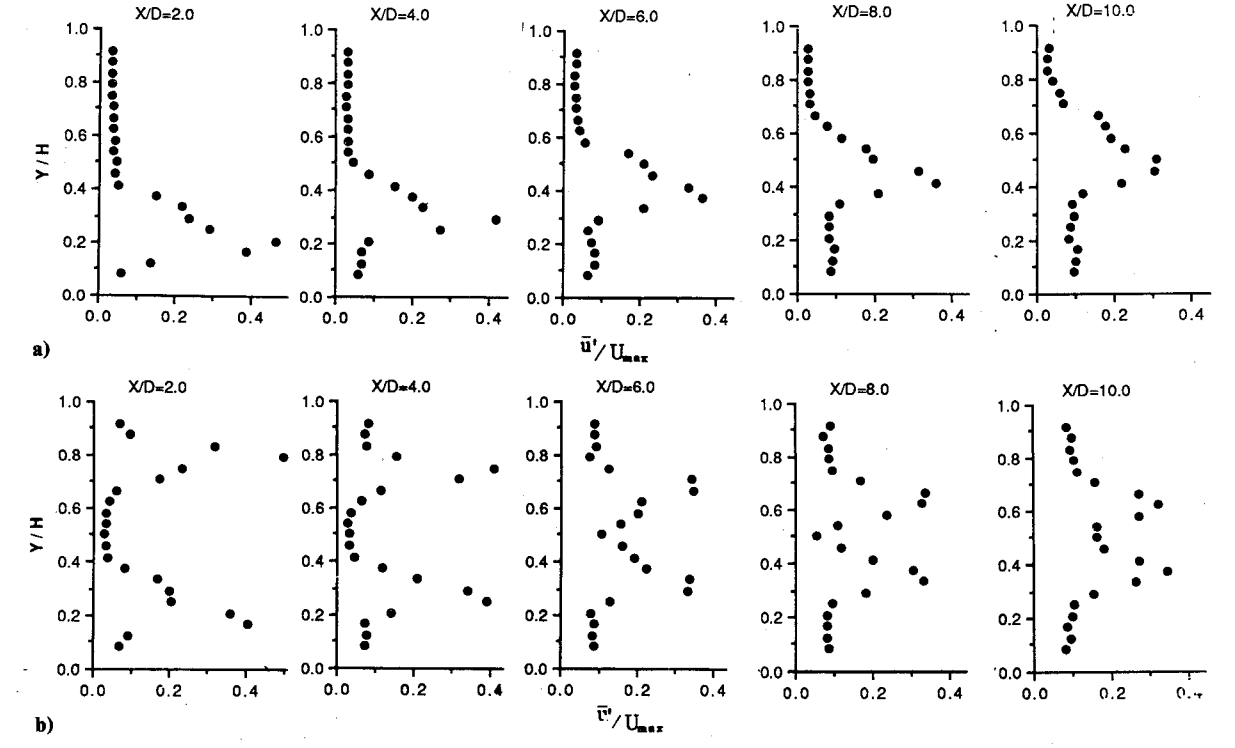

Fig. 9 Turbulent velocity profiles at $J = 25.2$: a) for one-line jet; b) for dual-line jets.

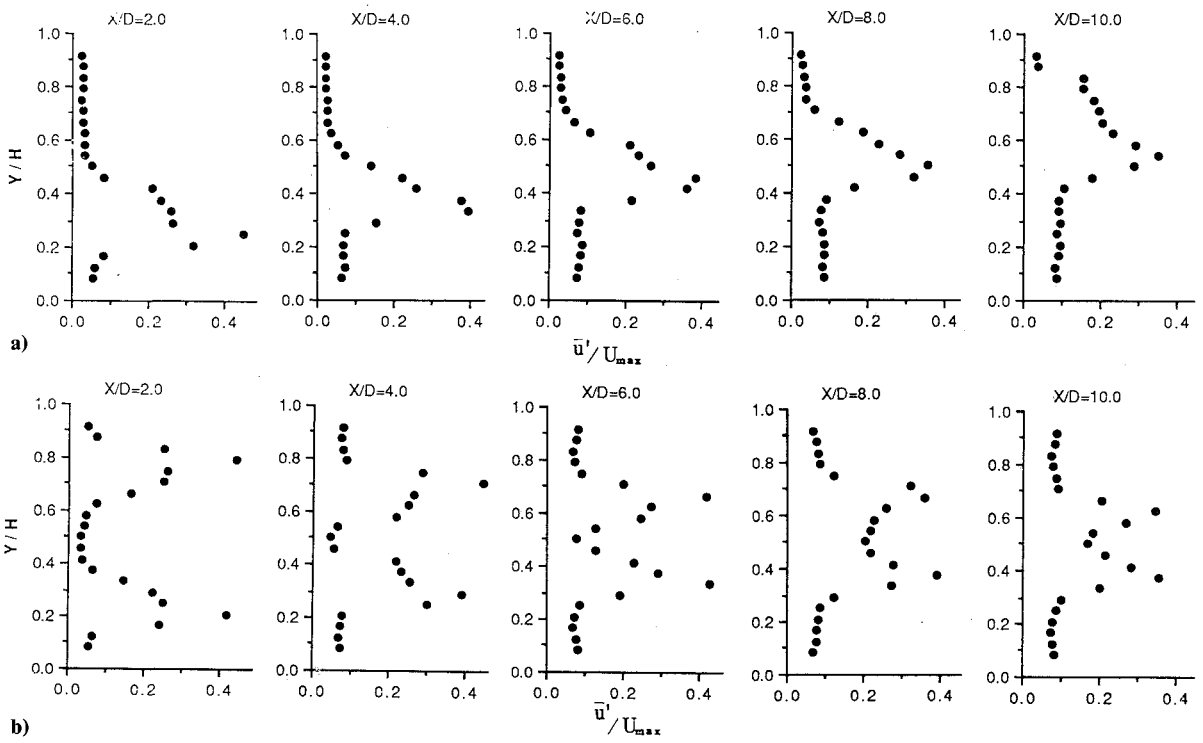

Fig. 10 Turbulent velocity profiles at $J = 50.4$: a) for one-line jet; b) for dual-line jets.

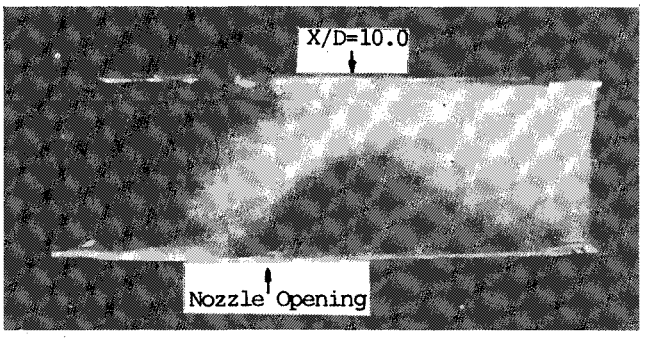

Fig. 11 Flow visualization result for one-line jet at $J = 17.3$.

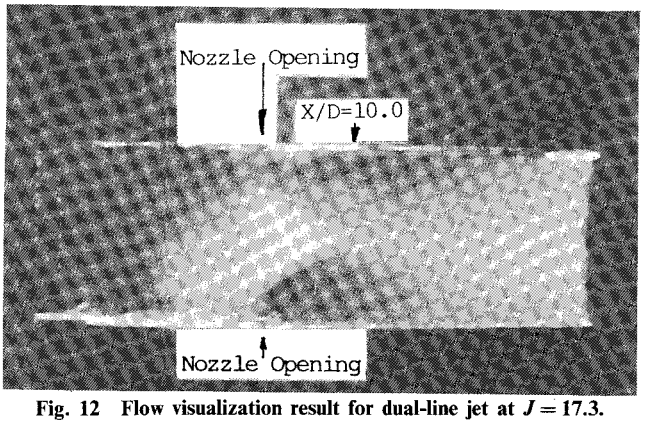

Fig. 12 Flow visualization result for dual-line jet at $J = 17.3$.

so-called "jet circulation depth," and the jet velocity trajectory Y_v is at the point where $\tilde{U} = \tilde{U}_{max}$. For example, for $X/D = 2.0$ in Fig. 6a, $Y_c/H = 0.18$ and $Y_v/H = 0.27$. It is seen from these figures that U drops quickly above Y_v/H to a value slightly above 0, and Y_v and Y_c both increase with increasing J and X/D.

For the dual in-line jets shown in Figs. 6b and 7b, the velocity profile is symmetric about the midheight $Y/H = 0.5$ at every X/D plane. There is also a circulation zone near each of the nozzle opening, and Y_v/D and Y_c/D both increase with increasing J and X/D. The correlation equations of Y_v/D are also listed in Tables 3 and 4 for one- and dual-line jets, respectively. Figure 8 shows the correlation curves for Y_v/D, which also appear to be parabolic lines.

Typical dimensionless X-component turbulent velocity profiles, $\bar{u}'/U_{max}$, at various X/D planes for $J = 25.2$ and 50.4 are shown in Figs. 9 and 10, respectively. It is seen from Figs. 9a and 10a for a one-line jet that turbulent velocity is strong within the region of $W^{\pm}_{1/2}$ (see Figs. 3a and 4a), and $\bar{u}'_{max}$ occurs at the position close to the jet velocity trajectory Y_v/D. As the mixing air moves far downstream, the Y/D value for the maximum turbulence intensity increases and the turbulent intensity appears to decay slowly.

For dual in-line jets shown in Figs 9b and 10b the turbulent velocity profile at every X/D plane is also symmetric about the channel midheight $Y/H = 0.5$, where u' is minimum. The turbulent velocity is also strong within the region of $W^{\pm}_{1/2}$ (see Figs. 3b and 4b), and turbulent intensity also decays slowly far downstream.

Flow Visualization

A typical flow visualization result for the one-line jet is shown in Fig. 11 for $J = 22.0$. It is seen from the figure that jet trajectory appears to be a parabolic line, and there is a circulation zone near the region of the nozzle opening. A typical visualization result for the dual in-line jets is shown in Fig. 12 for $J = 17.3$. It is seen that velocity field is essentially symmetric about the channel midheight. There is also a circulation zone near each of the nozzle opening, and the jet trajectory increases with the downstream distance X/D. All of the qualitative information depicted by the visualization results is in agreement with the measurements described previously.

Summary

An experimental study is presented for the mixing of one- and dual-line heated jets injected normally into a confined cold crossflow. Measurements of the mean temperature, velocity, and turbulence intensity together with the flow visualization have revealed the influences of the momentum flux ratio and downstream distance on the thermal and velocity

fields in the range of $15.2 \leq J \leq 60$, $2 \leq X/D \leq 10$, and $H/D = 24$. Dimensionless vertical temperature profiles can be expressed in self-similar forms. Correlation equations for various dependent parameter in terms of the momentum flux ratio and downstream distance are given. It shows that jet temperature and velocity trajectories, circulation depth, and jet half-width increase with increasing J and X/D.

LDV measurements show that the turbulence intensity is strong within the jet half-width region, and the maximum intensity occurs at the point very close to the jet velocity trajectory.

Further studies on the effects of nozzle width and the jet impinging angle would be helpful, in particular, for the design of dilution zone in gas turbine combustors.

Acknowledgment

Partial support of this work by the Science and Technology Coordination Council in Defence in Taiwan under Grants CS 76-0210-D110-01 and CS 77-0210-D110-04 is acknowledged.

References

[1]Callagan, E. E., and Ruggeri, R. S., "A General Correlation Temperature Profile Downstream of a Heated Air Jet Directed Perpendicular to an Air Stream," NACA TN-2466, April 1951.

[2]Ramsey, J. W., and Goldstein, R. T., "Interaction of a Heated Jet with a Deflecting Stream," American Society of Mechanical Engineers Paper 71-HT-2, 1971.

[3]Kamotani, Y., and Greber, I., "Experiments on a Turbulent Jet in a Cross Flow," *AIAA Journal*, Vol. 10, Nov. 1972, pp. 1425–1429.

[4]Kamotami, Y., and Greber, I., "Experiments on Confined Turbulent Jets in Cross Flow," NASA CR-2392, March 1974.

[5]Holdeman, J. D., Walker, R. E., and Kors, D. L., "Mixing of Multiple Dilution Jets with a Hot Primary Airstream for Gas Turbine Combustors," NASA TM X-71426, Nov. 1973.

[6]Walker, R. E., and Eberhardt, R. G., "Multiple Jet Study Data Correlations," NASA CR-134795, April 1975.

[7]Cox, G. B., Jr., "Multiple Jet Correlations for Gas Turbine Engine Combustor Design," *Journal of Engineering for Power*, Vol. 98, April 1976, pp. 265–273.

[8]Holdeman, J. D., and Walker, R. E., "Mixing of a Row of Jets with a Confined Crossflow," *AIAA Journal*, Vol. 15, Feb. 1977, pp. 243–249.

[9]Chen, K. S., Ku, A. C., and Hwang, J. Y., "An Experimental Study of the Mixing of Opposing Jets with Crossflow in Gas Turbine Combustors," National Science Council Rept. CS 77-0210-D110-04, Taiwan, June 1989.

[10]"Laboratory Methods of Testing Fans for Rating," AMCA, 1975.

[11]Johnson, D. A., Modarress, D., and Owen, F. K., "An Experimental Verification of Laser-Doppler Sampling Bias and its Correction," *Journal of Fluids Engineering*, Vol. 106, March 1984, pp. 5–12.